IOP Publishing Nanotechnology

Nanotechnology **29** (2018) 275703 (9pp) https://doi.org/10.1088/1361-6528/aabdc9

The indispensable role of the transversal spin fluctuations mechanism in laser-induced demagnetization of Co/Pt multilayers with nanoscale magnetic domains

Wei Zhang[1,2], Wei He[1,4], Li-Cong Peng[1,2], Ying Zhang[1], Jian-Wang Cai[1,2], Richard F L Evans[3], Xiang-Qun Zhang[1] and Zhao-Hua Cheng[1,2,4]

[1] State Key Laboratory of Magnetism and Beijing National Laboratory for Condensed Matter Physics, Institute of Physics, Chinese Academy of Sciences, Beijing 100190, People's Republic of China
[2] School of Physical Sciences, University of Chinese Academy of Sciences, Beijing 100049, People's Republic of China
[3] Department of Physics, The University of York, Heslington, York YO10 5DD, United Kingdom

E-mail: hewei@iphy.ac.cn and zhcheng@iphy.ac.cn

Received 8 January 2018, revised 29 March 2018
Accepted for publication 12 April 2018
Published 4 May 2018

Abstract

The switching of magnetic domains induced by an ultrashort laser pulse has been demonstrated in nanostructured ferromagnetic films. This leads to the dawn of a new era in breaking the ultimate physical limit for the speed of magnetic switching and manipulation, which is relevant to current and future information storage. However, our understanding of the interactions between light and spins in magnetic heterostructures with nanoscale domain structures is still lacking. Here, both time-resolved magneto-optical Kerr effect experiments and atomistic simulations are carried out to investigate the dominant mechanism of laser-induced ultrafast demagnetization in $[Co/Pt]_{20}$ multilayers with nanoscale magnetic domains. It is found that the ultrafast demagnetization time remains constant with various magnetic configurations, indicating that the domain structures play a minor role in laser-induced ultrafast demagnetization. In addition, both in experiment and atomistic simulations, we find a dependence of ultrafast demagnetization time τ_M on the laser fluence, which is in contrast to the observations of spin transport within magnetic domains. The remarkable agreement between experiment and atomistic simulations indicates that the local dissipation of spin angular momentum is the dominant demagnetization mechanism in this system. More interestingly, we made a comparison between the atomistic spin dynamic simulation and the longitudinal spin flip model, highlighting that the transversal spin fluctuations mechanism is responsible for the ultrafast demagnetization in the case of inhomogeneous magnetic structures. This is a significant advance in clarifying the microscopic mechanism underlying the process of ultrafast demagnetization in inhomogeneous magnetic structures.

Keywords: ultrafast spin dynamics, nanoscale magnetic domains structures, TRMOKE

(Some figures may appear in colour only in the online journal)

[4] Authors to whom any correspondence should be addressed.

1. Introduction

Ferromagnetic thin films with nanoscale domain structures have attracted considerable attention due to their potential to serve as low-power spintronic devices [1, 2]. In recent decades, domain wall motions driven by a magnetic field [3], as well as the current via the spin transfer torque [4] in Co/Pt multilayers with strong perpendicular magnetic anisotropy, have been extensively reported. Other techniques including the use of electric field [5], voltage-induced strain [6] and thermal gradient [7] have also been utilized to manipulate the nanoscale magnetic domain structures. The discovery of ultrafast demagnetization, first reported by Beaurepaire *et al* [8] in 1996, opened up new routes for manipulating magnetization on the sub-picosecond timescale. For instance, an important milestone from the studies of ultrafast spin dynamics is the observation that the ultrashort laser can directly switch the magnetic domains in ferrimagnetic GdFeCo [9] without an external field. This leads to the dawn of a new era in breaking the ultimate physical limit for the speed of magnetic switching and manipulation. Recently, such all-optical switching has been extended to ferromagnetic Co/Pt multilayers as well as FePt nanoparticles [10]. However, apart from the demonstrated potential technologies for heat-assisted magnetic recording, investigations into the fundamental interactions between spins, electrons and lattices far from equilibrium are still lacking in the case of Co/Pt heterostructures with nanoscale magnetic domain configurations.

Since 1996, significant progress has been made in understanding the microscopic mechanism of ultrafast spin dynamics, including the important role of spin–orbit coupling [11], the direct interaction between spins and photons [12], as well as the spin transport [13] in multilayer thin films. In hindsight, most of these reports have focused on magnetic media with single domain structures [14]. In the case of inhomogeneous magnetic domain structures, the spin transport between neighboring magnetic domains has been demonstrated with the advent of femtosecond-pulse x-ray sources [15, 16] in $[Co/Pd]_{30}$ multilayer films as well as in $[Co/Pt]_{16}$ structures. However, Moisan *et al* cannot exclude the contributions from local spin flip scattering [17] by means of time-resolved magneto-optical Kerr effect (TRMOKE). In fact, the local approach [18, 19] such as the plain three-temperature model (3TM) [8] qualitatively describes the intense laser induced temperature evolution of the electrons, lattice, and spins with time. Based on this model, the atomistic Landau–Lifshitz–Gilbert (LLG) method [20–22] with Langevin dynamics is capable of reproducing the rapid decrease in the magnetization observed in experiment. In this case, the ultrashort laser pulse excitation leads to a nonequilibrium divergence between the electron temperature, T_e, and lattice temperature, T_l. We treat the electron gas as the heat bath for the spin system. Moreover, the conserved spin angular momentum is transferred locally and represented by the phenomenological Gilbert damping parameter [23, 24]. This computational model ignores the specific angular momentum transfer channel, whilst it provides a straightforward way [25] to understand the physics underlying the temporal evolution of magnetization after laser pulse excitation.

Considering that a consensus is still lacking regarding the dominant mechanism responsible for ultrafast demagnetization in multilayers with nanoscale magnetic domains, in this paper, the ultrafast demagnetization curves dependent on the magnetic domain configuration have been obtained via TRMOKE experiments in Co/Pt multilayers. Both in experiment and atomistic spin dynamics simulations, laser-fluence-dependent ultrafast demagnetization curves have been produced to demonstrate the indispensable role of local spin angular momentum dissipation in the presence of magnetic domain configurations. The ultrafast demagnetization time τ_M, as functions of Gilbert damping, has been compared with atomistic spin dynamics simulation and longitudinal spin flip model. Based on this comparison, the explicit mechanism of local spin angular momentum dissipation in the case of inhomogeneous magnetic structures is illustrated clearly in the simulation model, which is a significant advance in understanding the ultrafast demagnetization mechanism in Co/Pt systems with magnetic domains structures.

2. Experimental

2.1. Experimental method

In this study, both the applied field and laser-fluence-dependent ultrafast demagnetization curves for Ta (5 nm)/Pt (2 nm)/$[$Co (0.4 nm)/Pt (0.7 nm)$]_{20}$/Pt (2.3 nm) multilayers have been achieved using the TRMOKE technique [14, 26]. A train of optical pulses with a wavelength of 780 nm, 55 fs duration and 100 nJ/pulse is generated at 5.2 MHz repetition rate by a Ti: sapphire oscillator (FEMTOLASER, XL-100). A 200 μm thickness BBO crystal was used to double the frequency of the femtosecond laser. The laser beam from the source is split into both 780 nm and 390 nm beams. We use the 780 nm laser as the pump pulse to excite the magnetic system out of equilibrium, while the 390 nm laser pulse was used as a probe beam to measure the subsequent magnetization dynamics with the timescale from sub-picosecond to nanosecond. The pump laser beam is much stronger than the probe with an intensity ratio of at least 20 for the lowest pump fluence. Both the pump and probe beam are incident along the normal axis (z-axis) of the sample. The detection geometry is only sensitive to the out-of-plane component of the magnetization, M_z. The pump and probe beams are focused onto the sample with spot diameters of $\sim$10 μm and $\sim$5 μm via a 20$\times$ objective lens, respectively.

2.2. The measurements of static properties and spin precession for Ta (5 nm)/Pt (2 nm)/$[$Co (0.4 nm)/Pt (0.7 nm)$]_{20}$/Pt (2.3 nm)

The sample used in this study is a 22 nm [Co (0.4 nm)/Pt (0.7 nm)$]_{20}$ multilayer thin film, grown at room temperature by dc magnetron sputtering [27]. As shown in figure 1, the hysteresis loop along the surface normal of the film is

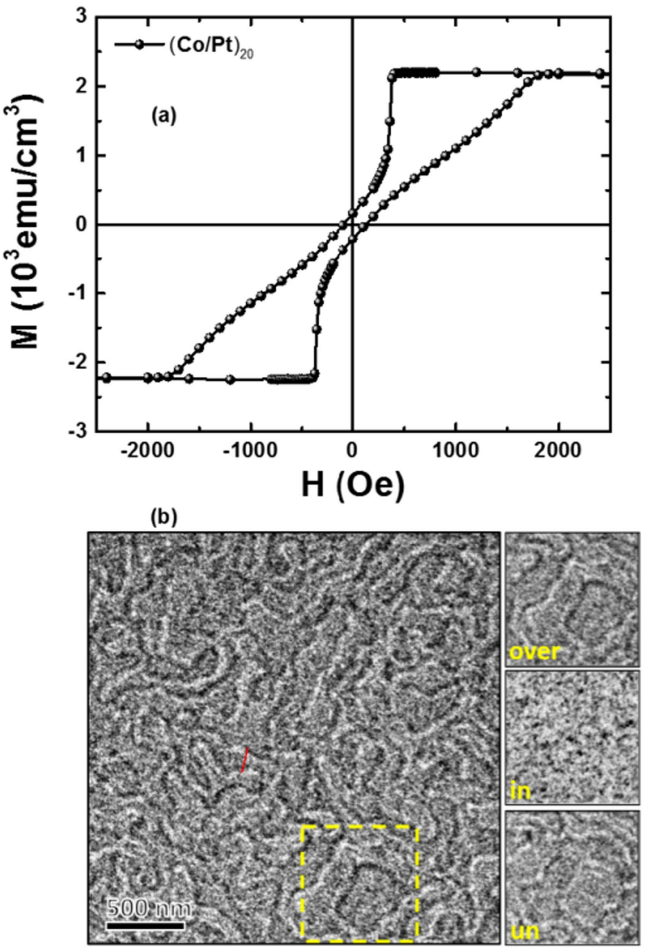

Figure 1. Static magnetic properties of Ta (5 nm)/Pt (2 nm)/[Co (0.4 nm)/Pt (0.7 nm)]$_{20}$/Pt (2.3 nm) multilayers. (a) The hysteresis loop along the perpendicular direction of the sample measured by a vibrating sample magnetometer, with the maximum applied fields of 4 kOe. (b) Lorentz TEM images measured at zero applied field. The side images are the zoom-in for the domain structure in the dashed yellow box. 'Un', 'in' and 'ov' represent 'under-focused', 'in-focus' and 'over-focused' L-TEM images, respectively.

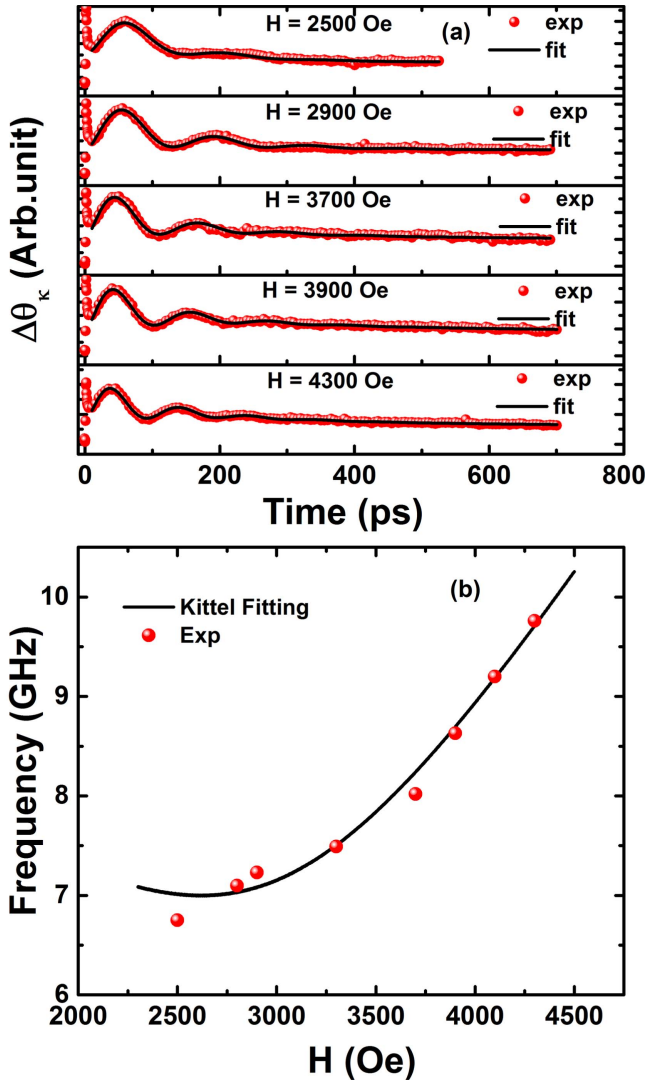

Figure 2. (a) Time-resolved magneto-optical Kerr effect (TRMOKE) signals for Ta (5 nm)/Pt (2 nm)/[Co (0.4 nm)/Pt (0.7 nm)]$_{20}$/Pt (2.3 nm) multilayers with applied fields H = 2500 Oe, 2900 Oe, 3700 Oe, 3900 Oe, 4300 Oe. (b) Magnetic field dependence of precession frequency with magnetic field applied at $\theta_H = 80°$ from the normal direction of the sample.

measured by a vibrating sample magnetometer. It is found that the Co/Pt multilayer exhibits an out-of-plane magnetic anisotropy, and an obvious jump in the loop occurs even before the applied field is reversed. The jump mainly comes from the onset of the domain formation, which is illustrated in figure 1(b) by the measurements taken using a Lorentz transmission electron microscope (L-TEM), showing the 260 nm domain structure.

To obtain the effective magnetic anisotropy, we performed the laser-induced magnetization precession experiment. In this case, the external field H, ranging from 2.5 kOe to 4.3 kOe, was applied at $\theta_H = 80°$ from the normal direction of the sample. The typical time-resolved magnetization dynamics with various applied fields shown in figure 2(a) can be fitted by the damped harmonic function added to an exponential decaying background [28]:

$$\Delta M(t) = A + B\exp(-\nu t) + C\exp\left(-\frac{t}{\tau}\right)\sin(2\pi f t + \varphi) \quad (1)$$

where A and B are the background magnitudes, and ν is the background recovery rate. c, τ, f and ϕ are the magnetization precession amplitude, relaxation time, frequency and phase, respectively. From the fitting curves shown in figure 2(a) (solid lines), the value of precession frequency f is extracted. Figure 2(b) shows the frequency as a function of applied field. The experimental $f - H$ relation can be fitted by an analytic Kittel formula derived from the LLG equation:

$$f = \frac{\gamma}{2\pi}\sqrt{H_1 H_2} \quad (2)$$

where $H_1 = H\cos(\theta_H - \theta) + H_K^{eff}\cos^2\theta$, $H_2 = H\cos(\theta_H - \theta) + H_K^{eff}\cos 2\theta$.

The equilibrium angle of magnetization was obtained from the relationship $\sin 2\theta = \frac{2H}{H_K^{eff}}\sin(\theta_H - \theta)$. The direction

of applied field is fixed at $\theta_H = 80°$. In the above equations, H_K^{eff} and γ are the effective perpendicular magnetization anisotropy and gyromagnetic ratio, respectively, where $H_K^{eff} = \frac{2K_{eff}}{M_s}$, $\gamma = \frac{2\pi g \mu_B}{h}$. In our calculation, the Lande g-factor was set to 2.2 as the bulk Co value, and the best fitting value of K_{eff} is 2.8×10^6 erg cm^{-3} for the $[Co/Pt]_{20}$ multilayer [29]. We take this value as the input parameter in the atomistic simulation below.

2.3. The measurements of ultrafast demagnetizaion curves for Ta (5 nm)/Pt (2 nm)/[Co (0.4 nm)/Pt (0.7 nm)]$_{20}$/Pt (2.3 nm)

In previous studies [15, 16], femtosecond-pulse x-ray sources have been used to demonstrate the acceleration effect of spin angular momentum transferring between neighboring domains on ultrafast demagnetization. This makes the role of magnetic domain structures played in ultrafast demagnetization interesting. In order to clarify the role played by spin transport in various domain configurations, we carried out the time-resolved MOKE measurements for different applied fields. When H is larger than 400 Oe, the sample is completely magnetized. As the applied fields are reduced from a saturated one of 900 Oe, the multidomain configurations gradually appear. Figure 3(a) shows the magnetization as a function of time delay for a series of magnetic domain configurations at a fixed incident laser fluence of 0.5 mJ cm^{-2}. We can clearly observe that the evolution of magnetization curves looks identical for various applied fields. The solid lines reproduce the experimental data obtained by the 3TM as follows [30]:

$$-\frac{\Delta M(t)}{M} = \left\{\left[\frac{A_1}{(t/\tau_0+1)^{0.5}} - \frac{(A_2\tau_E - A_1\tau_M)}{\tau_E - \tau_M}e^{-\frac{t}{\tau_M}} - \frac{\tau_E(A_1 - A_2)}{\tau_E - \tau_M}e^{-\frac{t}{\tau_M}}\right]\Theta(t) + A_3\delta(t)\right\} * G(t, \tau_G) \quad (3)$$

$G(t, \tau_G)$ represents the Gaussian laser pulse profile, whose full width at half maximum (FWHM) is τ_G. $\Theta(t)$ is a step function, $\delta(t)$ is the Dirac delta function. τ_M is defined as the time needed for magnetization to reach a level of $(1 - e^{-1})$ of its maximum demagnetization [24] and τ_E is the electron-phonon equilibration time, describing the rate at which electrons and phonons exchange their energy and reach a temperature equilibrium [31]. The parameter τ_0 represents the heat transport timescale through the substrates. In this model, the electrons absorb the laser photons directly, and then excite the hot electrons. Once the thermalization is produced by Coulomb interactions, the electrons, spins and phonons can be described by the three-temperature model. The relaxation takes place through energy transfer between different baths. Although it ignores the angular momentum transferring, the 3TM has been widely used to extract the ultrafast demagnetization time. Equation (3) is solved based on a set of differential equations (4) of the 3TMs by neglecting the spin

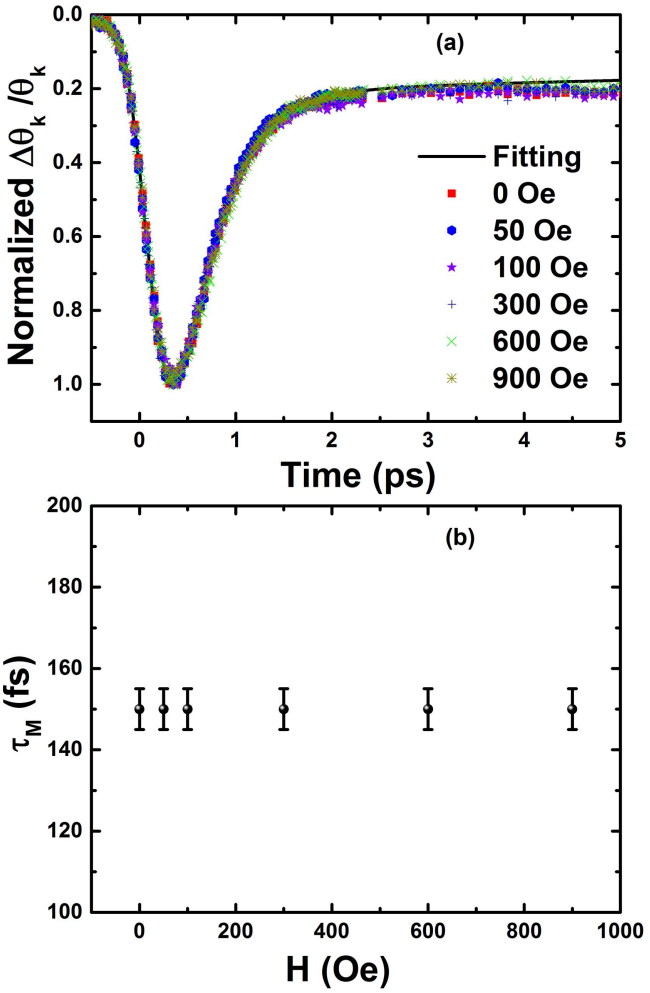

Figure 3. Ultrafast demagnetization curves and demagnetization time. (a) Ultrafast demagnetization curves as a function of applied fields with H = 0 Oe, 50 Oe, 100 Oe, 300 Oe, 600 Oe, 900 Oe. (b) Extracted demagnetization time as a function of applied fields.

specific heat in the low fluence limit [32].

$$C_e\frac{\partial T_e}{\partial t} = -G_{e-p}(T_e - T_p) - G_{e-s}(T_e - T_s) + P(t)$$
$$C_p\frac{\partial T_p}{\partial t} = -G_{e-p}(T_p - T_e) - G_{s-p}(T_p - T_s),$$
$$C_s\frac{\partial T_s}{\partial t} = -G_{e-s}(T_s - T_e) - G_{s-p}(T_s - T_p) \quad (4)$$

where C_e, C_p, C_s are the heat capacities of the electrons, lattices and spins, respectively. G_{e-p}, G_{e-s}, G_{s-p} are the electron-lattice, electron-spin and spin-lattice interaction constants, and P(t) represents the excitation from the laser pump pulse. Figure 3(b) shows that the demagnetization time τ_M is a constant value with various applied fields, indicating that there is no obvious influence by the domain structures on ultrafast demagnetization time. This is consistent with the TRMOKE experimental observation in both Co/Pd and Co/Pt multilayers with magnetic domains [17].

In the case of magnetic domain structures, the ultrafast demagnetization time τ_M induced by spin transport is independent of the laser fluence [15]. It is completely different

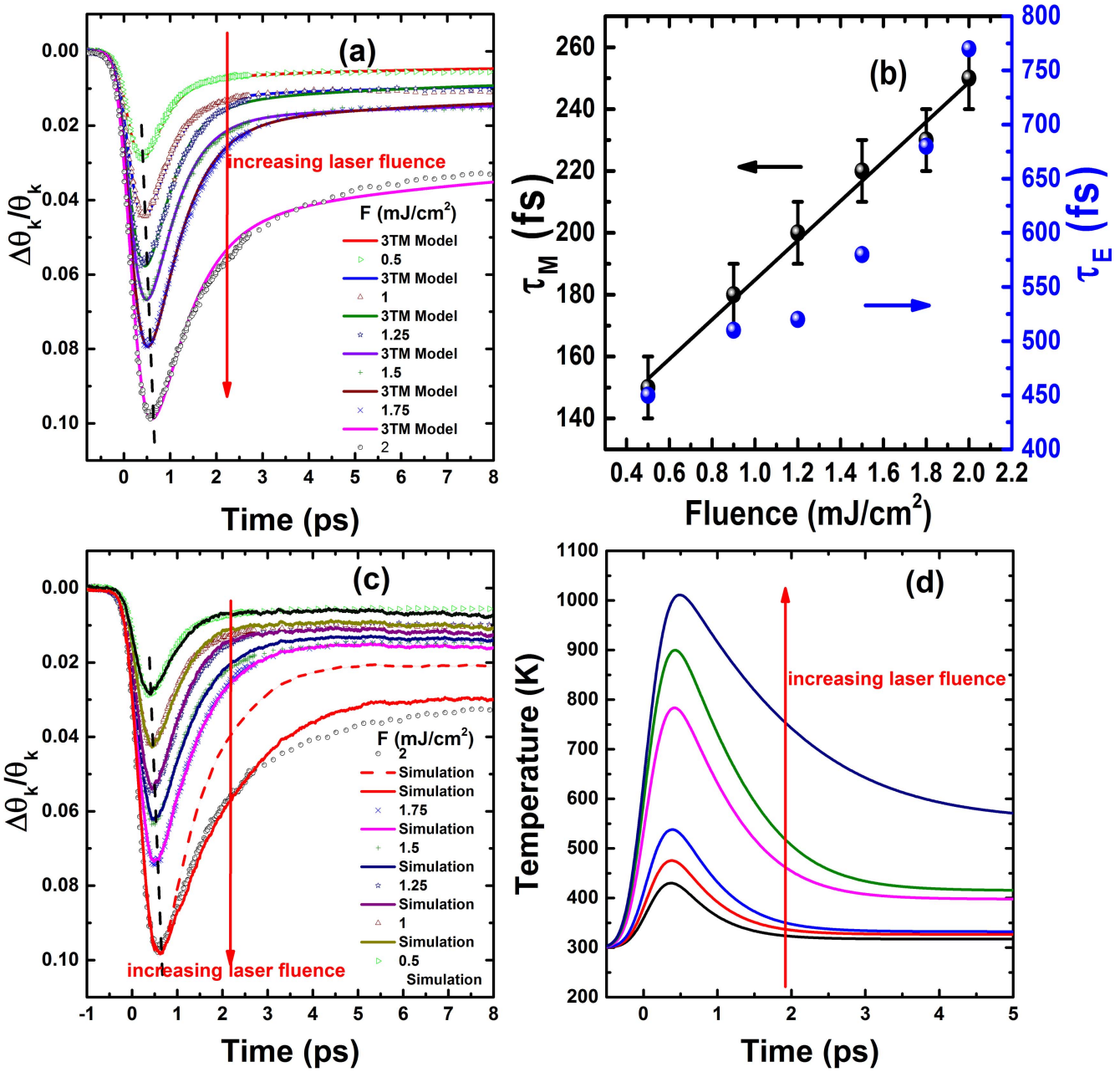

Figure 4. TRMOKE experimental and atomistic simulation results. (a) Ultrafast demagnetization curves with various laser fluences ranging from 0.5 mJ cm^{-2} to 2 mJ cm^{-2}. The solid lines represent the fitting data by the three temperature model (3TM). (b) Extracted demagnetization time from 3TM as well as recovery time as a function of laser fluences. (c) The experimental demagnetization curves reproduced by atomistic simulations indicated by the solid and dashed lines. The dashed red line is calculated using $\gamma = 3 \times 10^3$ J · m^{-3} · K^{-1}, while the solid red line results from $\gamma = 6.2 \times 10^3$ J · m^{-3} · K^{-1}. (d) The simulated time evolution of electron temperatures with various laser fluences.

from the previous results based on local spin-flip scattering [33, 34]. Therefore, we performed the time-resolved TRMOKE measurements as a function of laser fluence at $H = 50$ Oe, as shown in figure 4(a). We chose such a value of applied field because it leads to a multidomain state, as demonstrated in figure 1. It is obvious that the higher laser fluence gives rise to a longer time needed to demagnetize the sample as the maximum magnetic quenching increases. Because equation (3) is valid in the low fluence limit, the largest laser fluence used here is 2 mJ cm^{-2}. The demagnetization curves obtained in a laser fluence larger than 2 mJ cm^{-2} would not be reproduced well by equation (3), giving rise to the invalid value of demagnetization time τ_M. We have to address the fact that the critical value of the laser fluence differs largely within different systems. It is mainly due to the varying thermal conductivity of the samples [17]. Figure 4(b) reports the demagnetization time τ_M as well as τ_E, characterizing the magnetization recovery time extracted from the 3TM with various laser fluence. A nearly linear relation between the demagnetization time τ_M and laser fluence is

established. Moreover, the values of τ_M fall into the range of 150 $\sim$ 300 fs which agrees very well with that obtained in a 15 nm thick homogeneous Co film, where it was explained by Koopmans *et al* using an electron-phonon medicated spin-flip scattering model [35]. The high dependence on laser fluence of the demagnetization time provides further evidence that the spin-flip scattering dominates the ultrafast demagnetization in the present system. In addition, the recovery time τ_E of magnetization is slowed down obviously by increasing the laser fluence, agreeing with previous results [36] obtained by both experiment as well as microscopic Landau–Lifshitz–Bloch (LLB) calculations.

Our conclusions contrast with the previous demonstration in Co/Pt multilayers using femtosecond-pulse x-ray sources [15], in which the hot electrons displacement between neighboring domains plays a major role in the ultrafast demagnetization process. The different lifetimes as well as velocities between spin-majority and spin-minority hot electrons can induce an imbalance in spin accumulation in the region close to the domain wall, resulting in local magnetization quenching. The estimated spin-transport-induced domain wall broadening is around 20 nm [17]. Therefore, in the future, reducing both the spatial resolution of the laser source and the domain size in the samples can facilitate the exploration of spin dependent hot-electron transport in ferromagnets with nanoscale magnetic domains. However, the explicit mechanism of local spin angular momentum dissipation in such an inhomogeneous system with nanoscale magnetic domains has never been mentioned so far. This is the central strategy in this paper.

3. Atomistic spin dynamics model

3.1. Simulation method

The atomistic spin dynamics simulation [20, 21] was performed using the VAMPIRE software to investigate the microscopic mechanism underlying ultrafast demagnetization. In this atomistic simulation, the spin Hamiltonian $\mathfrak{I}$ of the systems are described by an extended Heisenberg spin model with the following form:

$$\mathfrak{I} = -\sum_{i\neq j} J_{ij}\vec{S_i}\cdot\vec{S_j} - K_{eff}\sum_i(\vec{S_i}\cdot\vec{e})^2 - \sum_i \mu_s\vec{S_i}\cdot\overrightarrow{H_{app}} \quad (5)$$

The first term is the Heisenberg exchange energy, where $J_{ij} = 6.064 \times 10^{-24}\, J/link$ is the exchange interaction constant between the nearest neighboring two spins α and $\vec{S_j}$. The second term describes the magnetocrystalline anisotropy of the spin, where $K_{eff} = 1.1 \times 10^{-24}$ J/atom is the effective uniaxial magnetic anisotropy constant induced mainly by the Co/Pt interface. The last term is the Zeeman energy involving interactions between the system and external applied fields, where $\mu_s = 1.72\mu_B$ is the magnetization moment per atom. The dynamics of spin systems are determined by the LLG equation with Langevin dynamics:

$$\frac{\partial\vec{S_i}}{\partial t} = -\frac{\gamma}{(1+\lambda^2)}[\vec{S_i}\times\overrightarrow{H^i{}_{eff}} + \lambda\vec{S_i}\times(\vec{S_i}\times\overrightarrow{H^i{}_{eff}})] \quad (6)$$

where γ is the gyromagnetic ratio and λ is the microscopic Gilbert damping parameter mainly coming from intrinsic contributions of spin-electron and spin-lattice interactions. $\overrightarrow{H^i{}_{eff}}$ is the net magnetic field on each spin including an additional white noise term:

$$\overrightarrow{H^i_{th}} = \Gamma(t)\sqrt{\frac{2\lambda k_B T}{\gamma\mu_s\Delta t}},$$

where k_B is the Boltzmann constant, T is the temperature of the electron system, Δt is the integration time step, and $\overrightarrow{\Gamma(t)}$ is the Gaussian white noise term representing the thermal fluctuations on each atomic site. So, the effective field in the LLG equation with Langevin dynamics reads:

$$\overrightarrow{H^i_{eff}} = -\frac{1}{\mu_s}\frac{\partial\mathfrak{I}}{\partial\vec{S_i}} + \overrightarrow{H^i_{th}}$$

The electron system temperature is calculated from a two-temperature model [20]:

$$\begin{aligned} C_e\frac{\partial T_e}{\partial t} &= -G_{e-p}(T_e - T_p) + P(t) \\ C_p\frac{\partial T_p}{\partial t} &= -G_{e-p}(T_p - T_e) \end{aligned} \quad (7)$$

where C_e, C_p are the electron and lattice heat capacities, respectively. T_e is the electron temperature, T_p is the lattice (phonon) temperature, G_{e-p} is the electron-lattice coupling constant, and the parameter $P(t)$ is determined by a Gaussian pulse with height proportional to the effective laser fluence via the relationship

$$P(t) = F_{eff}\cdot e^{-\frac{(t-3t_0)^2}{t_0{}^2}}, \quad (8)$$

where F_{eff} is the effective laser fluence parameter without dimension and t_0 is the duration of the laser pulse. The time evolution of the electron temperature is solved using a simple Euler scheme.

In the numerical simulation carried out by VAMPIRE, we assume that the heat capacity of lattice C_p is independent of the lattice temperature and given by $C_p = 8.5 \times 10^6$ J · m^{-3} · K^{-1}, while the electronic heat capacity C_e is taken as proportional to the temperature T_e via $C_e = \gamma T_e$ with $\gamma = 3 \times 10^3$ J · m^{-3} · K^{-1}. The value of electron-lattice coupling parameter G_{e-p} is set as 1.5×10^{18} W · m^{-3} · K^{-1}. The values of all the parameters are consistent with those in the literature [8, 23, 32]. In addition, the value of effective laser fluence F_{eff} was increased from 6×10^{20} to 5×10^{21} monotonously in the numerical calculations to reproduce the experimental curves with laser fluence increasing from 0.5 mJ cm^{-2} to 2 mJ cm^{-2} in figure 4(a).

3.2. Simulation results and discussions

To demonstrate the indispensable role of the local spin angular momentum dissipation in this system, atomistic

simulations were carried out to reproduce the laser-fluence-dependent experimental curves. As shown in figure 4(c), we can clearly observe that the experimental curves are reproduced exactly within the atomistic spin model by increasing the laser power, justifying the local spin angular momentum dissipation suffices here and explaining the ultrafast demagnetization. In the case of $F = 2\,\mathrm{mJ\,cm^{-2}}$, the simulation result, shown as the dashed red line, disagrees with the experimental curve. This discrepancy can be attributed to the nonlinear temperature dependence of electronic heat capacity in reality, which always takes place at high laser fluence [37]. However, this effect is ignored in the current simulation model. In this case, a larger value of $\gamma = 6.2 \times 10^3\,\mathrm{J \cdot m^{-3} \cdot K^{-2}}$ could be used in the simulation to reproduce the experimental curve, as is shown by the solid red line in figure 4(c). On the other hand, the effect of heat accumulation is more pronounced as the laser fluence is increased. It can be demonstrated as the recovery time τ_E increases with increasing laser fluence in figure 4(b). However, such an effect is also not considered in the simulation model, which may be another reason for the deviation of the simulated result from the experimental one. Despite this, the atomistic calculations reproduce the main features in the TRMOKE experiment, namely, an increase in the demagnetization time is needed when the loss of magnetization increases. As shown in figure 4(d), the increasing laser fluence results in an increase in the electron temperature. The higher electron temperature leads to a larger maximal demagnetization. Consequently, a longer relaxation time is needed to demagnetize the system.

In the present atomistic spin model, the microscopic damping parameter [20] λ, which represents the local intrinsic contributions from spin-lattice and spin electrons interactions, is used to account for the local spin angular momentum transfer to induce ultrafast demagnetization. To highlight the microscopic mechanism responsible for ultrafast demagnetization in the present system, we address the relationship between ultrafast demagnetization time and the microscopic Gilbert damping parameter, since both of them require a transfer of angular momentum from the electronic system to the lattice. In the case of 3*d* transition metal cobalt, shown as the dotted line in figure 5(a), at a given laser fluence, we can clearly note that the maximum magnetic quenching increases as the microscopic Gilbert damping parameter increases, while the demagnetization time reduces. In fact, the microscopic Gilbert damping parameter λ coming from the local intrinsic contributions (spin-lattice and spin-electron interactions) in the atomistic spin dynamics model, as the bridge between the spins and the heat baths of electrons and phonons, represents the strength of the spin–orbit coupling effect [38]. Therefore, it is expected that a larger microscopic Gilbert damping, λ, can make the demagnetization faster and larger, as shown in figure 5(a). This agrees qualitatively with the prediction given by phonon-mediated spin-flip scattering, where the spin–orbit coupling effect induces the spin mixing probability [39] and consequently the spin flip scattering.

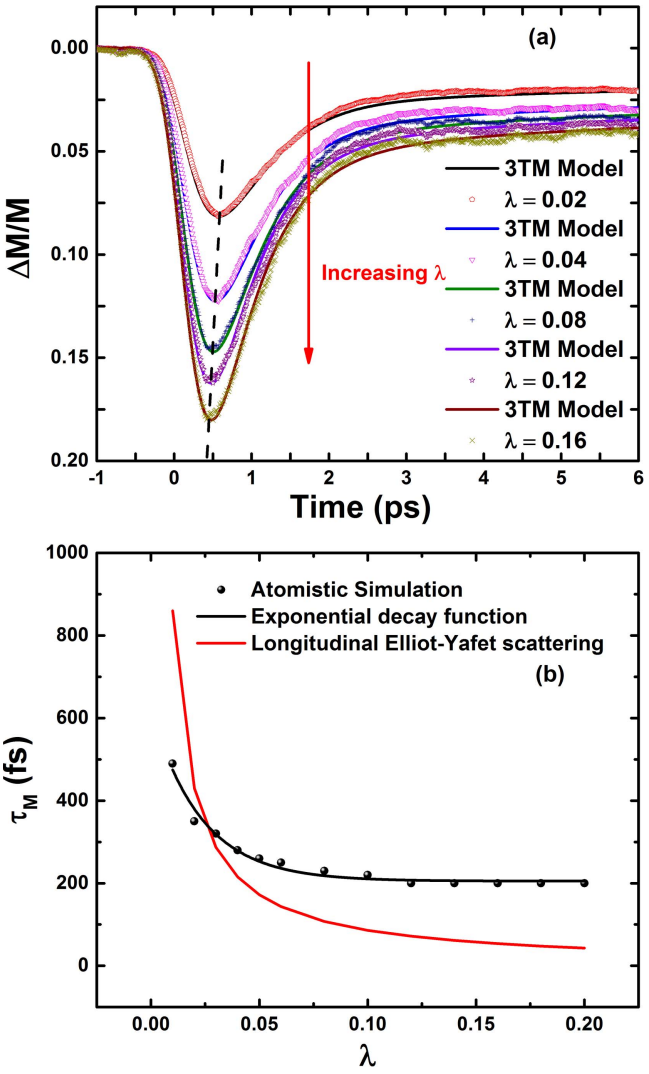

Figure 5. Atomistic simulation results for Co film. (a) Ultrafast demagnetization curves with various microscopic damping values fitted by the 3TM (solid lines). (b) The black dots represent the demagnetization time extracted from atomistic simulations as a function of microscopic damping constant. The exponential decay fitting is represented by the black line, while the results obtained by Koopmans *et al* are represented by the red line.

Despite this agreement, to illustrate the mechanism of ultrafast demagnetization in the framework of atomistic simulations, figure 5(b) highlights the difference in ultrafast demagnetization time, τ_M, between the atomistic simulations and the longitudinal spin flip model by Koopmans *et al* [19], as functions of the microscopic Gilbert damping λ. In the case of the longitudinal spin flip model, an inverse relation between τ_M and λ, shown as the red line in figure 5(b), has been derived via the Curie temperature T_c, $\tau_M = C_0 \frac{h}{2\pi K_B T_c \lambda}$, with h and K_B the Plank and Boltzmann constants, respectively. $C_0 = \frac{1}{4}$ is a constant value determined by Elliot–Yafet type scattering [19]. The atomistic simulation results are fitted by the 3TM and shown as the solid lines in figure 5(a), from which we extract the value of the demagnetization time. The extracted demagnetization time τ_M as a function of λ is shown

in figure 5(b) as the black dots. An exponential function is used to reproduce the relationship between τ_M and λ obtained from the atomistic simulations and indicates a more gradual change in the ultrafast demagnetization time with Gilbert damping compared with that given by longitudinal spin-flip scattering (phonon-mediated Elliot–Yafet type), shown as the red line in figure 5(b). The difference mainly comes from the fact that the transverse spin fluctuations determine the ultrafast demagnetization in the atomistic spin dynamics simulations, where the length of the local spin moment is fixed. This is in contrast to the model used by Koopmans *et al*, in which the magnitude of atomic moment is reduced by longitudinal spin-flips in Elliot–Yafet scattering events [35]. In fact, it has been demonstrated by TRMOKE experiments [40] as well as spin-resolved two-photo-photoemission techniques [41], that transverse spin fluctuations [22] are a possible explanation for ultrafast demagnetization.

Indeed, Atxitia *et al* [36] also reported a similar inverse relation between λ and τ_M within the micromagnetic LLB model. The LLB equation treats both transverse and longitudinal fluctuations of the atomic magnetic moments. It contains two parameters, a transverse and a longitudinal relaxation parameter which are both related to the intrinsic coupling-to-the-bath parameter, λ. This coupling parameter can be related to the actual matrix elements for spin-flip scattering. In contrast, only the transverse relaxation is involved in the atomistic LLG model used in this study. Despite this, the consistent results obtained in both LLB and LLG equations indicate that the phenomenological equations applied both at micromagnetic and atomistic scales contain the physics of ultrafast demagnetization behavior. Due to the lack of contributions from longitudinal relaxation to ultrafast demagnetization in the atomistic spin model, the comparison was made between the atomistic spin model and the longitudinal spin flip model by establishing the explicit relationship between the Gilbert damping constant and ultrafast demagnetization time. Thereby, we propose that transversal spin fluctuations are responsible for the ultrafast demagnetization mechanism in the current system.

4. Conclusions

In this study, laser induced ultrafast demagnetization dynamics in $[Co/Pt]_{20}$ multilayers with magnetic domain configurations have been studied using both TRMOKE experiments and atomistic spin dynamics simulations. It is found experimentally that the demagnetization time, τ_M, retains a constant value of 150 fs with various magnetic domain structures, showing that the spin-dependent hot electron transport between neighboring domains plays a minor role in ultrafast demagnetization in our samples. Moreover, the experimental evidence for a local spin-flip scattering mechanism, namely, that the demagnetization time increases as the laser fluence increases, is reproduced exactly by an atomistic spin dynamics simulation based on the model of local spin angular momentum dissipation. Via the atomistic spin dynamics model, the transversal spin fluctuations mechanism has been demonstrated to be responsible for the ultrafast demagnetization in the case of Co/Pt multilayers with inhomogeneous magnetic structures. This is a significant advance in clarifying the microscopic mechanism underlying the ultrafast demagnetization in inhomogeneous magnetic structures.

Acknowledgments

This work is supported by the National Key Research Program of China (Grant Nos. 2015CB921403, 2016YFA0300701, and 2017YFB0702702), the National Natural Sciences Foundation of China (Grant Nos. 91622126, 51427801, and 51671212) and the Key Research Program of Frontier Sciences, CAS (Grant Nos. QYZDJ-SSW-JSC023, KJZD-SW-M01 and ZDYZ2012-2).

ORCID iDs

Wei Zhang https://orcid.org/0000-0001-9635-5540
Li-Cong Peng https://orcid.org/0000-0002-8580-2285
Ying Zhang https://orcid.org/0000-0001-5476-1524
Richard F L Evans https://orcid.org/0000-0002-2378-8203

References

[1] Parkin S S P, Hayashi M and Thomas L 2008 Magnetic domain-wall racetrack memory *Science* **320** 190–4
[2] Allwood D A, Xiong G, Faulkner C C, Atkinson D, Petit D and Cowburn R P 2005 Magnetic domain-wall logic *Science* **309** 1688–92
[3] Metaxas P J, Jamet J P, Mougin A, Cormier M, Ferre J, Baltz V, Rodmacq B, Dieny B and Stamp R L 2007 Creep and flow regimes of magnetic domain-wall motion in ultrathin Pt/Co/Pt films with perpendicular anisotropy *Phys. Rev. Lett.* **99** 217208 -4
[4] Moore T A, Miron I M, Gaudin G, Serret G, Auffret S, Rodmacq B, Schuhl A, Pizzini S, Vogel J and Bonfim M 2008 High domain wall velocities induced by current in ultrathin Pt/Co/AlO_x wires with perpendicular magnetic anisotropy *Appl. Phys. Lett.* **93** 262504 -3
[5] Schellekens A J, van den Brink A, Franken J H, Swagten H J M and Koopmans B 2012 Electric-field control of domain wall motion in perpendicularly magnetized materials *Nat. Commun.* **3** 847 -5
[6] Shepley P M, Rushforth A W, Wang M, Burnell G and Moore T A 2015 Modification of perpendicular magnetic anisotropy and domain wall velocity in Pt/Co/Pt by voltage-induced strain *Sci. Rep.* **5** 7921–5
[7] Moretti S, Raposo V, Martinez E and Lopez-Diaz L 2017 Domain wall motion by localized temperature gradients *Phys. Rev.* B **95** 064419 -10
[8] Beaurepaire E, Merle J C, Daunois A and Bigot J Y 1996 Ultrafast spin dynamics in ferromagnetic nickel *Phys. Rev. Lett.* **76** 4250–3
[9] Stanciu C D, Hansteen F, Kimel A V, Kirilyuk A, Tsukamoto A, Itoh A and Rasing T 2007 All-optical magnetic recording with circularly polarized light *Phys. Rev. Lett.* **99** 047601–4
[10] Lambert C H *et al* 2014 All-optical control of ferromagnetic thin films and nanostructures *Science* **345** 1337–40

[11] Zhang G P and Hübner W 2000 Laser-induced ultrafast demagnetization in ferromagnetic metals *Phys. Rev. Lett.* **85** 3025–8

[12] Bigot J Y, Vomir M and Beaurepaire E 2009 Coherent ultrafast magnetism induced by femtosecond laser pulses *Nature Phys.* **5** 515–20

[13] Battiato M, Carva K and Oppeneer P M 2010 Superdiffusive spin transport as a mechanism of ultrafast demagnetization *Phys. Rev. Lett.* **105** 027203–4

[14] Zhang W, He W, Zhang X Q, Cheng Z H, Teng J and Fähnle M 2017 Unifying ultrafast demagnetization and intrinsic Gilbert damping in Co/Ni bilayers with electronic relaxation near the Fermi surface *Phys. Rev.* B **96** 220415(R)–7

[15] Vodungbo B *et al* 2012 Laser-induced ultrafast demagnetization in the presence of a nanoscale magnetic domain network *Nat. Commun.* **3** 999

[16] Pfau B *et al* 2012 Ultrafast optical demagnetization manipulates nanoscale spin structure in domain walls *Nat. Commun.* **3** 1100–6

[17] Moisan N, Malinowski G, Mauchain J, Hehn M, Vodungbo B, Luning J, Mangin S, Fullerton E E and Thiaville A 2014 Investigating the role of superdiffusive currents in laser induced demagnetization of ferromagnets with nanoscale magnetic domains *Sci. Rep.* **4** 4658

[18] Haag M, Illg C and Fähnle M 2014 Role of electron-magnon scatterings in ultrafast demagnetization *Phys. Rev.* B **90** 014417

[19] Koopmans B, Ruigrok J J M, Dalla Longa F and de Jonge W J M 2005 Unifying ultrafast magnetization dynamics *Phys. Rev. Lett.* **95** 267207

[20] Evans R F L, Ostler T A, Chantrell R W, Radu I and Rasing T 2014 Ultrafast thermally induced magnetic switching in synthetic ferrimagnets *Appl. Phys. Lett.* **104** 082410–4

[21] Evans R F L, Fan W J, Chureemart P, Ostler T A, Ellis M O A and Chantrell R W 2014 Atomistic spin model simulations of magnetic nanomaterials *J. Phys. Condens. Matter* **26** 103202–24

[22] Kazantseva N, Nowak U, Chantrell R W, Hohlfeld J and Rebei A 2008 Slow recovery of the magnetisation after a sub-picosecond heat pulse *Europhys. Lett.* **81** 27004–6

[23] Atxitia U and Chubykalo-Fesenko O 2011 Ultrafast magnetization dynamics rates within the Landau–Lifshitz-Bloch model *Phys. Rev.* B **84** 144414

[24] Kuiper K C, Roth T, Schellekens A J, Schmitt O, Koopmans B, Cinchetti M and Aeschlimann M 2014 Spin–orbit enhanced demagnetization rate in Co/Pt multilayers *Appl. Phys. Lett.* **105** 202402

[25] Ostler T A *et al* 2012 Ultrafast heating as a sufficient stimulus for magnetization reversal in a ferrimagnet *Nat. Commun.* **3** 666–71

[26] He W, Zhu T, Zhang X Q, Yang H T and Cheng Z H 2013 Ultrafast demagnetization enhancement in CoFeB/MgO/CoFeB magnetic tunneling junction driven by spin tunneling current *Sci. Rep.* **3** 2883–7

[27] Wu Q, He W, Liu H L, Liu Y F, Cai J W and Cheng Z H 2013 Magnetization reversal asymmetry in [Co/Pt]/CoFe/IrMn multilayers with enhanced perpendicular exchange bias *J. Appl. Phys.* **113** 033901

[28] Song H S, Lee K D, Sohn J W, Yang S H, Parkin S S P, You C Y and Shin S C 2013 Relationship between Gilbert damping and magneto-crystalline anisotropy in a Ti-buffered Co/Ni multilayer system *Appl. Phys. Lett.* **103** 022406

[29] Song H S, Lee K D, Sohn J W, Yang S H, Parkin S S P, You C Y and Shin S C 2013 Observation of the intrinsic Gilbert damping constant in Co/Ni multilayers independent of the stack number with perpendicular anisotropy *Appl. Phys. Lett.* **102** 102401–5

[30] Malinowski G, Longa F D, Rietjens J H H, Paluskar P V, Huijink R, Swagten H J M and Koopmans B 2008 Control of speed and efficiency of ultrafast demagnetization by direct transfer of spin angular momentum *Nat. Phys.* **4** 855–8

[31] Dalla Longa F, Kohlhepp J T, de Jonge W J M and Koopmans B 2007 Influence of photon angular momentum on ultrafast demagnetization in nickel *Phys. Rev.* B **75** 224431–4

[32] Dalla Longa F 2008 Laser-induced magnetization dynamics *PhD Thesis* Eindhoven University of Technology

[33] Roth T, Schellekens A J, Alebrand S, Schmitt O, Steil D, Koopmans B, Cinchetti M and Aeschlimann M 2012 Temperature dependence of laser-induced demagnetization in Ni: a key for identifying the underlying mechanism *Phys. Rev.* X **2** 021006–7

[34] Hohlfeld J, Matthias E, Knorren R and Bennemann K H 1997 Nonequilibrium magnetization dynamics of nickel *Phys. Rev. Lett.* **78** 4861–4

[35] Koopmans B, Malinowski G, Dalla Longa F, Steiauf D, Fähnle M, Roth T, Cinchetti M and Aeschlimann M 2010 Explaining the paradoxical diversity of ultrafast laser-induced demagnetization *Nat. Mater.* **9** 259–65

[36] Atxitia U, Chubykalo-Fesenko O, Walowski J, Mann A and Münzenberg M 2010 Evidence for thermal mechanisms in laser-induced femtosecond spin dynamics *Phys. Rev.* B **81** 174401–8

[37] Atxitia U 2012 Modeling of ultrafast laser-induced magnetization dynamics within the Landau–Lifshitz-Bloch approach *PhD Thesis* Instituto de Ciencia de Materiales de Madrid

[38] Stohr J and Siegmann H C 2012 *Magnetism: From Fundamentals to Nanoscale Dynamics* (Berlin: Springer) 586–7

[39] Fähnle M and Illg C 2011 Electron theory of fast and ultrafast dissipative magnetization dynamics *J. Phys. Condens. Matter* **23** 493201–18

[40] Carpene E, Mancini E, Dallera C, Brenna M, Puppin E and De Silvestri S 2008 Dynamics of electron-magnon interaction and ultrafast demagnetization in thin iron film *Phys. Rev.* B **78** 174422–6

[41] Schmidt A B, Pickel M, Donath M, Buczek P, Ernst A, Zhukov V P, Echenique P M, Sandratskii L M, Chulkov E V and Weinelt M 2010 Ultrafast magnon generation in an Fe film on Cu (100) *Phys. Rev. Lett.* **105** 197401–4